Highly efficient and stable spray assisted nanostructured Cu_2S/Carbon paper counter electrode for quantum dots sensitized solar cells

Gurpreet S. Selopal [a,b], Ralph Chahine [b], Mahyar Mohammadnezhad [b], Fabiola Navarro-Pardo [a,b], Daniele Benetti [b], Haiguang Zhao [c,**], Zhiming M. Wang [a,***], Federico Rosei [a,b,*]

[a] Institute of Fundamental and Frontier Sciences, University of Electronic Science and Technology of China, Chengdu, 610054, PR China
[b] Centre for Energy, Materials and Telecommunications, Institut National de La Recherche Scientifique, 1650 Boulevard Lionel-Boulet, Varennes, Quebec, J3X 1S2, Canada
[c] College of Physics and State Key Laboratory of Bio-Fibers and Eco-Textiles, Qingdao University, No. 308 Ningxia Road, Qingdao, 266071, PR China

HIGHLIGHTS

- The spray deposition approach was used to fabricate efficient and stable Cu_2S/CP CE.
- Cu_2S/CP CEs offer low series resistance and high catalytic activity.
- QDSC based on Cu_2S/CP CEs yield a 28% higher PCE than the brass CEs.
- A PCE of 5.89% can be obtained upon the optimization of the photoanode structure.

GRAPHICAL ABSTRACT

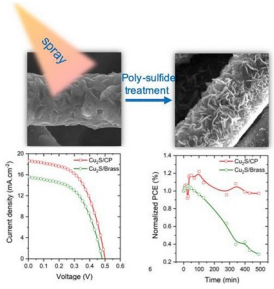

ARTICLE INFO

Keywords:
Cu_2S nanostructures
Carbon fiber paper
Quantum dots
Counter electrode
Quantum dot-sensitized solar cells

ABSTRACT

The counter electrode (CE) plays a significant role in determining the overall performance and long-term stability of quantum dots (QDs) sensitized solar cells (QDSCs) by collecting the electrons from the external circuit and catalyzing the regeneration of the oxidized electrolyte. In this work, we report a simple, low cost and large area scalable spray deposition approach to fabricate nanostructured Cu_2S CE on a carbon fiber paper (CP). The QDSCs were assembled with optimized spray assisted nanostructured Cu_2S/CP CEs, and yield a photoconversion efficiency (PCE) of 5.06%, which is 28% higher than QDSCs based on Cu_2S/Brass CEs. The PCE can be further boosted to 5.89% upon optimization of the photoanode structure. In addition, QDSCs with Cu_2S/CP CEs exhibit better long-term stability than QDSCs with Cu_2S/Brass CE. This excellent performance and satisfactory long-term stability of QDSCs with Cu_2S/CP CEs is mainly attributed to the synergistic effect of excellent conductivity of CP and high and stable catalytic activity of nanostructured Cu_2S, which is confirmed by cyclic voltammetry and electrochemical impedance spectroscopy. Thus, our results define a cost-effective and large area scalable

* Corresponding author. Centre for Energy, Materials and Telecommunications, Institut National de La Recherche Scientific,1650 Boulevard Lionel-Boulet, Varennes, Quebec, J3X 1S2, Canada.
** Corresponding author. College of Physics and State Key Laboratory of Bio-Fibers and Eco-Textiles, Qingdao University, No. 308, Ningxia Road, Qingdao, 266071, PR China.
*** Corresponding author.Institute of Fundamental and Frontier Sciences, University of Electronic Science and Technology of China, Chengdu, 610054, PR China.
E-mail addresses: hgzhao@qdu.edu.cn (H. Zhao), zhmwang@uestc.edu.cn (Z.M. Wang), rosei@emt.inrs.ca (F. Rosei).

approach to fabricate highly efficient and stable CEs, which is an important step toward the fabrication of solar driven optoelectronic devices.

1. Introduction

Quantum dot sensitized solar cells (QDSCs) [1] belong to the third-generation photovoltaic devices and are considered as a promising alternative to commercially available silicon solar cells. QDSCs possess the possibility to boost the photoconversion efficiency (PCE) beyond the Shockley–Queisser limit of 32.7% [2,3] due to the appealing optoelectronic properties of QDs such as size/composition-tunable absorption [4], high absorption coefficient [5], large intrinsic dipole moments [6], the possibility of multiple exciton generation (MEG) [7] and hot electron extraction before thermalization [8]. In the past few years, the record PCE of liquid-junction QDSCs improved significantly from 3% to 12.07% by exploiting engineered colloidal QDs as sensitizer [9–11], suitable electrolyte composition [12,13] and new counter electrode (CE) materials such as Ti-mesh supported mesoporous carbon [14], nitrogen-doped mesoporous carbon (N-MC) [15] and graphene hydrogel based nanostructures [16]. The CE is an important component of QDSCs and plays a critical role in determining the performance as well as the long-term stability of QDSCs by collecting the electrons from the external circuit and regeneration of the oxidized polysulfide electrolyte at the CE/electrolyte interface [17]. Thus, an efficient and fast regeneration of the oxidized polysulfide electrolyte reduces the back-electron transfer rate at the photoanode and speeds up the oxidized QDs regeneration. Hence the structure and composition of the CE strongly affects the overall functional performance of QDSCs [18]. The ideal CE should have high electrical conductivity, high specific surface area with high catalytic activity and chemical stability surrounding polysulfide electrolyte medium [19–21].

Over the past few years, considerable efforts have been devoted to fabricating CEs with the above-mentioned characteristics. Hodes et al. [22], demonstrated that metal sulfides (Cu, Co, Ni and Pb) materials possess excellent characteristics to be applied as efficient cathodes for the polysulfide electrolyte to replace conventional noble metal-based CEs [23–25]. Among such systems, copper sulfide (Cu_2S or CuS) with band gap of 1.1–1.4 eV, exhibits superior catalytic activity and stability in polysulfide electrolyte and are widely studied as efficient CE materials in QDSCs compared to the other materials [9–12,26]. Brass foil and fluorine doped tin oxide (FTO) glass are the most commonly used substrates to fabricate CEs for QDSCs [27–29]. The Cu_2S CEs based on HCl treated brass foil substrate suffers from chemical stability issues, due to the corrosion on the brass surface by polysulfide electrolyte during long-term use, which limits long-term application [26,29,30]. The CEs deposited on FTO glass substrates such as spray assisted Cu_2S [29], PbS [31], Cu_3Se_2 [32], etc. exhibit poor performance due to low conductivity (high series resistance), which reduces the fill factor (*FF*) and the open circuit voltage (V_{oc}) and hence the overall PCE of the QDSCs [33]. During the last few years, low dimensional carbonaceous materials (carbon nanotubes, graphene, carbon black, mesoporous carbon) [34–37] and their composites with chalcogenide metal sulfides [38–41] have been widely used to fabricate efficient electrode for solar energy conversion and energy storage devices.

More recently, a mesoporous carbon supported by Ti-mesh substrate has been used as CE for QDSCs. These devices exhibited a certified PCE of 11.16% by using CdSeTe QDs as light harvester [14], which was further boosted to 12.07% by using Zn-Cu-In-Se QDs sensitized photoanodes and N-MC carbon as CE [15]. However, the methodologies adopted in these works to fabricate the CEs are quite complicated and time-consuming and difficult to scale up. Therefore, there is an urgent need to seek an alternative simple, fast and large area scalable approach to fabricate CEs with low cost, high catalytic activity and long-term stable features for the construction of efficient and stable QDSCs. In this context, spray pyrolysis is a simple, low cost and versatile technique, suitable for preparing large area CEs under ambient conditions, which is crucial for the industrial scale production of QDSCs [29,42]. In addition, the size and morphology of as synthesized nanostructures can be efficiently controlled by spray pyrolysis parameters such as flow rate, substrate-to-nozzle distance, carrier gas pressure, substrate temperature and concentration of solutions [43].

Herein, we report a simple, low cost and large area scalable two-step spray deposition approach to fabricate Cu_2S CEs on carbon fiber paper (CP), see Scheme 1. The CP is used as substrate and is composed of interconnected carbon fibers, which provides a three-dimensional (3D) network for fast electron transfer to catalytic active Cu_2S nanostructured generated over the carbon fiber. In addition, CP offers lower sheet resistance due to high conductivity and superior chemical stability in a polysulfide electrolyte. QDSCs fabricated by using spray assisted nanostructured Cu_2S/CP as CE with CdS/CdSe cascade QDs as light absorbers yield a high PCE of 5.09%, which is 28% higher than the PCE of QDSCs fabricated with Cu_2S/Brass CEs. This higher value of the PCE is mainly attributed to a low series resistance and high electrocatalytic activity of spray assisted nanostructured Cu_2S/CP CE as compared to Cu_2S/Brass CE.

2. Experimental section

2.1. Chemicals

Copper nitrate trihydrate (≥98%), cadmium acetate dihydrate (≥99%), sodium sulfide nonahydrate (≥99.9%), sodium borohydride (≥96%), ethanol (≥99.8%) and methanol (≥99.9%) were purchased from Sigma Aldrich. Thiourea (Assay = 99.0%) and zinc acetate dihydrate (99.999%) were purchased from Fluka. All chemicals were used as received without further purification.

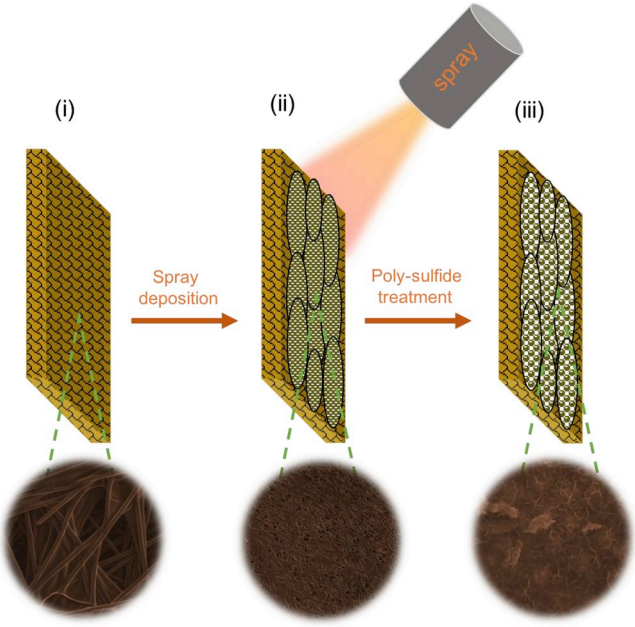

Scheme 1. Schematic diagram and SEM images of the preparation of nanostructured Cu_2S based CE: (i) Carbon fiber paper (CP); (ii) Spray deposited Cu_2S film on CP; (iii) Polysulfide treated nanostructured Cu_2S on CP.

2.2. Cathode preparation

2.2.1. Spray assisted Cu_2S

The spray deposition technique was used to prepare Cu_2S/CP CEs. The mixture of aqueous solutions of 0.1 M $Cu(NO_3)_2 \times 3H_2O$ and 0.05 M $CS(NH_2)_2$, was sprayed on ultrasonically cleaned CP maintained at 315 °C; the nozzle-to-substrate distance was set at 30 cm; pressure of gas carrier (N_2) was 10 psi. The spray duration was 10 s, with a 10 s pause in between two successive spray cycles. A series of Cu_2S/CP CEs were prepared with different number of spray cycles to uncover the best performing conditions.

2.2.2. Cu_2S/brass

Cu_2S/Brass CEs were prepared by treating the brass sheet into HCl (13 M) at 70 °C for 10–15 min to active the surface. The change in color from yellow to light pink confirms the complete treatment of brass. Cu_2S nanostructured CEs were generated by treating the HCl treated brass with polysulfide electrolyte for 10 min (see Fig. 1S). The surface color changes from light pink to black due to the formation of Cu_2S active species.

2.2.3. Platinum/FTO

Platinum/FTO CEs with thickness of 5 nm were prepared on FTO substrates under argon atmosphere by RF magnetron sputtering (Kurt J. Lesker, CM818).

2.3. Anode preparation

A thin and compact TiO_2 blocking layer was deposited on ultrasonically cleaned FTO glass substrates by hydrolysis of 0.50 mM $TiCl_4$ solution at 70 °C for 30 min. It was then annealed at 500 °C for 30 min under ambient atmosphere and left to cool down to room temperature. Double layer mesoporous TiO_2 anodes were prepared by doctor blading the transparent TiO_2 paste composed of small 20 nm in diameter (18 NR-T from Dyesol) on top of the compact TiO_2 layer. A drying process was followed for 15 min at ambient conditions, then placed on a hot plate for 6 min at 120 °C. Subsequently, a scattering layer of anatase TiO_2 nanoparticles (150-250 nm-sized, WER2-O) was then deposited on the above prepared transparent layer under the same conditions [27]. All the photoanodes were then annealed at 500 °C for 30 min under ambient conditions. The thickness of all photoanodes was measured by profilometer and an average value of 12μm was found for all the photoanodes.

2.4. QDs deposition

QDs were directly grown over the TiO_2 mesoporous films by a successive ionic layer absorption and reaction (SILAR) and chemical bath deposition (CBD). For CdS QDs, a 0.05 M ethanolic solution of Cd $(CH_2COO)_2{\cdot}2H_2O$ was used as Cd^{2+} source and 0.05 M solution of $Na_2S{\cdot}9H_2O$ in methanol/water (50:50 V:V) was used as S^{2-} source. For one SILAR cycle, 1 min dipping of photoanodes in metallic cation precursor (Cd^{2+}) followed by washing in the corresponding solvent to remove the chemical residuals from the surface followed by drying with N_2, followed by 1 min dipping in sulfur precursor (S^{2-}) and finally washed in the corresponding solvent to remove the chemical residuals from the surface and then dried with N_2. After CdS QDs deposition, a ZnS capping layer was formed through four SILAR cycles under the same conditions as for CdS QDs. For ZnS deposition, Zn^{2+} ions were deposited from 0.1 M methanolic solution of $Zn(CH_3COO)_2{\cdot}2H_2O$, whereas the S^{2-} ions were deposited from 0.1 M mixed solution (1:1 methanol: water) of $Na_2S{\cdot}9H_2O$. For CdSe QDs, the CBD solution was prepared by using 0.1 M Na_2SeSO_3, 0.1 M $Cd(CH_3COO)_2$, and 0.2 M $N(CH_2COONa)_3$ with a volume ratio of 1:1:1 [44]. The CdS QDs (5 SILAR cycles) sensitized TiO_2 mesoporous film was immersed in the solution for 3 h under dark conditions at room temperature and washed with ethanol to remove unabsorbed precursors. Finally, a ZnSe capping layer was deposited on CdS/CdSe cascade QDs sensitized TiO_2 mesoporous film by three SILAR cycles. For ZnSe capping layer deposition, first the photoanodes were immersed in 0.1 M Zn $(CH_3COO)_2$ and then washed with methanol and dry with N_2. Then Se^{2-} ions were deposited from the mixed solution of 0.03 M ethanolic solution of Se and a 0.06 M $NaBH_4$ under N_2 and washed with ethanol. To further boost the performance of QDSCs, one batch of samples were prepared by deposition of additional ZnSe layer prior to QDs deposition through two SILAR cycles of ZnSe, without altering the cascade structure of CdS/CdSe QDs [45].

2.5. Device fabrication

QDSCs were fabricated by sandwiching the QD sensitized TiO_2 photoanode and the spray assisted nanostructured Cu_2S/CP CE between 25 μm plastic spacers. Prior to device fabrication, the Cu_2S/CP CEs were treated with the polysulfide electrolyte for 10 min, so as to generate Cu_2S active species. Polysulfide in H_2O/methanol (1/1 v/v) (1 M Na_2S, 1 M S and 0.1 M NaOH) was used as an electrolyte. The CP, Cu_2S/Brass and Platinum/FTO were also used as CEs for the reference.

2.6. Characterization

Scanning electron microscopy (SEM, JEOL JSM-6900 F) was used to study the morphology of the as-prepared Cu_2S/CP and polysulfide electrolyte treated Cu_2S/CP CE at different magnifications. Chemical composition mapping of as prepared Cu_2S/CP and polysulfide treated Cu_2S/CP CE was carried out by energy dispersive X-ray spectroscopy (EDS). The XPS spectra of as-prepared Cu_2S/CP and polysulfide treated Cu_2S/CP CEs were measured in a VG Escalab 220i-XL equipped with a hemispherical analyzer, applying a Twin Anode X-Ray Source. The C 1s peak (BE = 284.8 eV) was used as an internal reference to rule out charging effects. The fine structure of the spectra was treated using Casa XPS software (2.3.15Version). TEM measurements were carried out by using a JEOL 2100F TEM coupled with selected area electron diffraction (SAED). Cyclic voltammetry (CV) was conducted in a Solartron SI 1287 potentiostat/galvanostat, using a three-electrode cell, using the Cu_2S/CP, Cu_2S/Brass, CP or Platinum/FTO as the working electrode saturated, a Platinum Plate as counter electrode and a Ag/AgCl reference electrode and polysulfide electrolyte (10 times diluted) using a 20 mV s^{-1} scan rate. The current-voltage (*I-V*) and transient photovoltage decay measurements were carried out using a compact solar simulator class AAA (Sciencetech SLB-300A) under one sun simulated sunlight (1 sun = AM 1.5G, 100 mWcm^{-2}), calibrated with a silicon reference cell.

Electrochemical impedance spectroscopy (EIS) was carried under dark conditions by using a SOLARTRON 1260 A Impedance/Gain-Phase Analyzer with zero bias voltage. All impedance measurements were analysed using an appropriate equivalent circuit model with Z-View software (v3.5, Scribner Associate, Inc.).

3. Results and discussion

3.1. Structural and chemical surface characterizations

Fig. 1 (a)-(f) displays the SEM images of as-prepared CE and after polysulfide treatment at different magnifications. The results demonstrated that the CP is homogeneously covered after three spray cycles (10s spray with 10 s pauses in between two successive spray cycles) [Fig. 1 (a)]. At higher magnification, each carbon fiber of CP is covered with one dimensional (1D) nanostructure with length in the range of 2–3 μm [Fig. 1 (b)] and each 1D branch is composed of small sized nanoparticles [Fig. 1 (c)]. After the treatment of as-prepared CE with 2 M polysulfide for 10 min, CE undergoes morphological and chemical changes due to the reaction between Cu_2SO_4 nanostructure and polysulfide. Hybrid nanostructures are formed, which are composed of self-assembled nanosheets with lateral dimensions in the range of 100–200nm [Fig. 1 (e)-(f)]. This self-assembled hierarchical structure

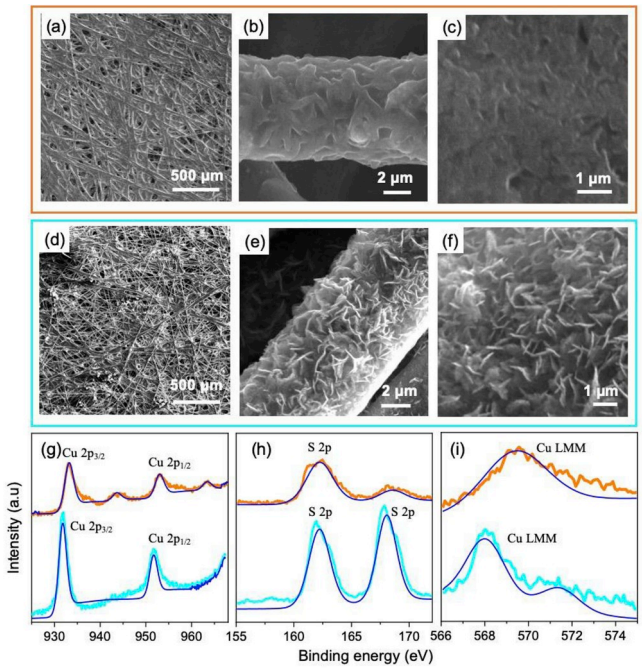

Fig. 1. SEM images of spray deposited Cu_2S film on CP at different magnifications: (a)–(c) As-prepared; (d)–(f) polysulfide treated Cu_2S film. Comparison of high resolution XPS of analysis of as-prepared Cu_2S film (Orange line) and after 10 min polysulfide treated (Cyan line) with fitting (blue line): (g) Cu 2p; (h) S 2p; (i) Cu LMM Auger peak. (For interpretation of the references to color in this figure legend, the reader is referred to the Web version of this article.)

offers high specific surface area and highly active catalytic sites, which are required for better catalytic action of the CEs [29].

The surface of as received brass is smooth with slight scratches [Fig. 1S (a)-(c)]. After the HCl treatment, there are slight morphological changes [Fig. 1S (d)-(f)]. The hierarchical structures of Cu_2S are formed on the surface of brass subsequent to 10min polysulfide treatment, which are mainly composed of self-assembled sheets with lateral size of 100–200 nm [Fig. 1S (g)-(i)]. Fig. 2S displays the SEM images of the Platinum/FTO CEs before [Fig. 2S (a)-(c)] and after the treatment with polysulfide [Fig. 2S (d)-(f)]. However, it is difficult to visualize the poisoning effect of the polysulfide electrolyte on Platinum/FTO due to very thin layer of Pt film (~5 nm).

XPS spectra were acquired to determine the chemical composition of the as-prepared CE and after the treatment with polysulfide. Fig. 1 (g)-(i) shows the comparison of the composition of the as-prepared CE and after treatment with polysulfide. The XPS spectra of as-prepared CEs shows peaks at 933.1 eV and 953.1 eV, corresponding to Cu $2p_{3/2}$ and $2p_{1/2}$, respectively and additional shake-up peaks observed at 943.7 eV and 963.4 eV in the spectral region of Cu 2p, which confirm the presence of Cu(II) in $CuSO_4$ [Fig. 1 (g)] [24]. The S 2p spectrum shows a main peak at 162.4 eV and a small peak at 168.4 eV, which confirms the presence of S^{-2} [Fig. 1 (h)]. Furthermore, the Cu LMM auger peak at 569.5 confirms that the Cu (II) is the main ion present [46]. Similarly, after the treatment with polysulfide CE shows morphological (as discussed above) and chemical changes. The polysulfide electrolyte treated CEs, shows the Cu $2p_{3/2}$ and $2p_{1/2}$ peaks at 931.9 eV and 951.6 eV respectively without shake-up contributions [Fig. 1 (g)] with slight changes in the Cu LMM peak position at 568.6 eV [Fig. 1 (i)], which confirms the presence of Cu (I) in polysulfide treated CEs. The analysis of S 2p shows two peaks at 161.8 eV and 167.8 eV confirming the formation of Cu_2S [Fig. 1 (h)] [47]. Thus, the polysulfide treatment of the as-prepared CE confirms the formation of Cu_2S having hierarchical nanostructure.

Fig. 2 (a) displays the XRD pattern of CP and polysulfide treated spray deposited Cu_2S/CP CE. The CP shows two sharp peaks at 27° and 55°, corresponding to (002) and (004) planes respectively [48] and a small broader peak at 43°. The XRD pattern of polysulfide treated spray deposited Cu_2S/CP CE exhibits new diffraction peaks centered at 27.1°, 37.4°, 45.2° and 54.1° corresponding to (002) (102) and (110) planes, respectively, which confirm the hexagonal structure of Cu_2S [17]. There are some additional peaks also observed at 14.3°, 16.1°, 19.5°, 28.8° and 31.6° corresponding to (004), (121), (212), (135) and (044) planes respectively, which are attributed to the face centered orthorhombic phase of non-reacted sulfur in the polysulfide electrolyte treated Cu_2S/CP CE.

To further investigate the crystal structure of the Cu_2S/CP CEs, high resolution TEM (HR-TEM) images and SAED patterns were recorded.

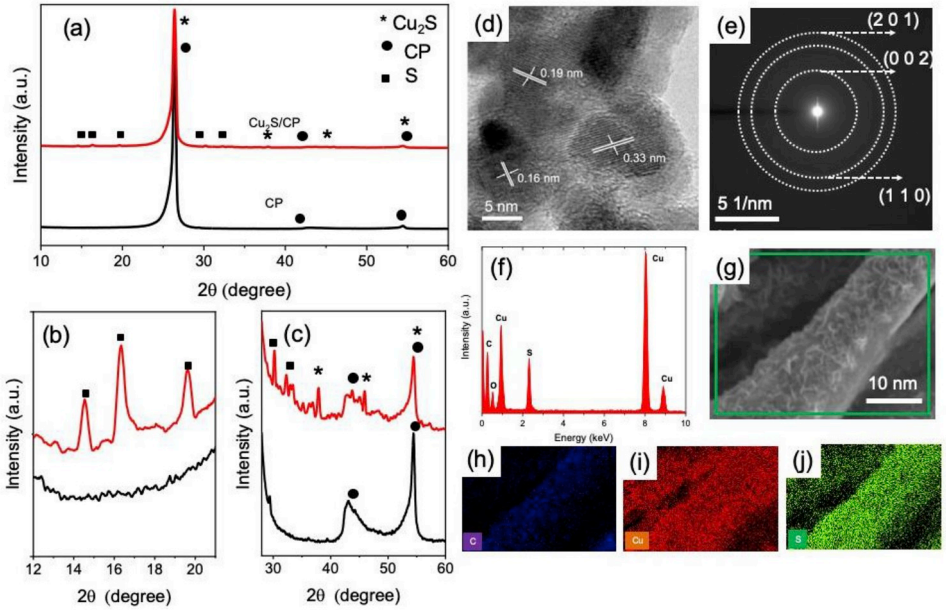

Fig. 2. (a) XRD of CP (black line) and polysulfide treated Cu_2S/CP CE (red line) and (b)–(c) magnified scale to highlight the peaks of Cu_2S nanostructure. Polysulfide treated Cu_2S film on CP: (d) High resolution TEM analysis; (e) SAED image; (f) EDS; (g) Elemental mapping by EDS spectroscopy; (h) carbon; (i) cupper; (j) sulfur. (For interpretation of the references to color in this figure legend, the reader is referred to the Web version of this article.)

Fig. 2 (d) displays an HR-TEM image, which clearly reveals the lattice fringes with inter-planar spacing of 1.94 Å, 3.34 Å and 1.65 Å corresponding to the (110), (002) and (201) planes of the hexagonal phase of Cu_2S (JCPDS 026–1116) respectively. The SAED patterns of the corresponding sample displayed in Fig. 2 (e). The calculated lattice parameters tabulated as (002), (110) and (201) planes of hexagonal phase of Cu_2S (JCPDS 026–1116). These findings are consistent with HR-TEM and XRD results. EDS analysis of the corresponding sample is shown in Fig. 2 (f), which confirms the presence of Cu and S as the main content. The XRD patterns of reference CEs: Platinum/FTO and Cu_2S/Brass are shown in Fig. 4S. The Platinum/FTO pattern shows peaks centered at 39.7°, 46.2°, 67.4° and 81.2°, corresponding to (111), (200) (220) and (311) planes respectively, confirming the face-centered cubic phase of Platinum/FTO (JCPDS 00-004-0802). Similarly, the Cu_2S/Brass pattern shows peaks at 27.7°, 32.1°,39.6°, 46.1° and 54.6°, corresponding to (111), (200), (211), (220) and (311) planes respectively, confirming the cubic phase of Cu_2S/Brass (JCPDS 00-053-0522).

The EDS elemental mapping of the selected rectangular area (green rectangle) in Fig. 2 (g) of polysulfide treated Cu_2S/CP CE is displayed in Fig. 2 (h)-(j). This confirms the homogeneous coverage of each carbon fiber of CP by Cu_2S nanostructures composed of Cu and S elements. This is consistent with the elemental analysis of Cu_2S/CP CE by TEM measurements [Fig. 2 (f)]. For the comparative study, we also performed elemental mapping of bare CP and spray assisted Cu_2S/CP before the polysulfide treatment (see Fig. 5S).

3.2. *Photovoltaic performance of QDSCs with different CEs*

To investigate the effect of spray deposition conditions on the performance of the Cu_2S CEs, a series of Cu_2S CEs were prepared by changing the number to spray cycles, while maintaining the other parameters of spray deposition constant such as carrier gas pressure, distance between the substrate and spray nozzle, substrate temperature and spray and pause time duration. QDSCs were fabricated using five SILAR cycles CdS QDs sensitized TiO_2 mesoporous photoanodes as a benchmark with Cu_2S CEs of one cycle, two, three and four cycles of spray deposition. Fig. 3 (a) shows the current density vs. voltage curves of QDSCs assembled with different types of Cu_2S/CP CEs. The functional

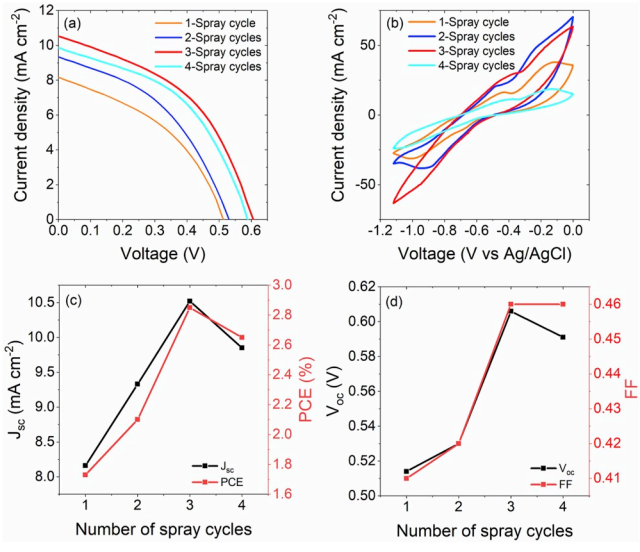

Fig. 3. (a) Current density vs voltage curves of QDSCs under one sun illumination based on spray deposited Cu_2S CEs prepared by different spray conditions. (b) CV analysis of corresponding Cu_2S CEs. Variation of functional parameters of QDSCs based on different Cu_2S CEs: (c) J_{sc} (mA.cm^{-2}) (black square) and *PCE* (%) (red square).; (d) V_{oc} *(V)* (black square) and *FF* (red square). (For interpretation of the references to color in this figure legend, the reader is referred to the Web version of this article.)

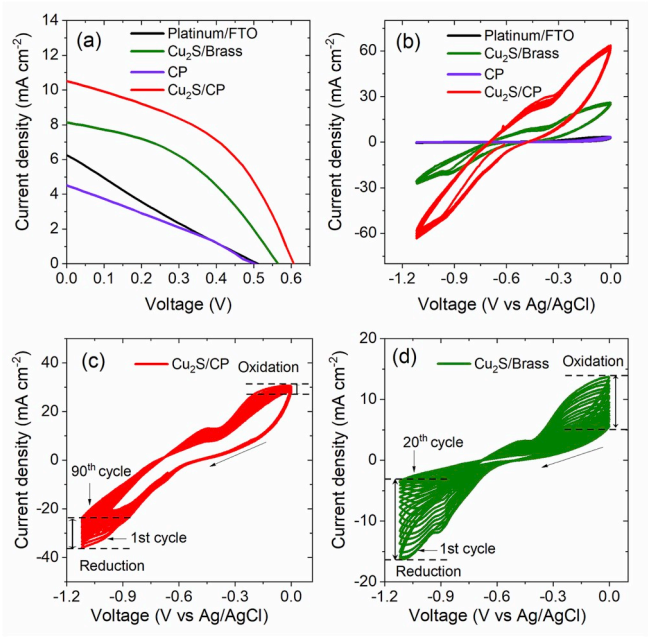

Fig. 4. (a) Current density vs voltage curves of QDSCs under one sun illumination based on different types of CEs: black line (Platinum/FTO); violet line (CP); green line (Cu_2S/Brass) and red line (spray deposited Cu_2S/CP, 3 cycles). (b) CV analysis of corresponding counter electrodes with scan rate 50 mV/s. Stability of counter electrodes vs number of CV cycles with scan rate 20 mV/s: (c) spray deposited Cu_2S/CP; (d) Cu_2S/Brass. (For interpretation of the references to color in this figure legend, the reader is referred to the Web version of this article.)

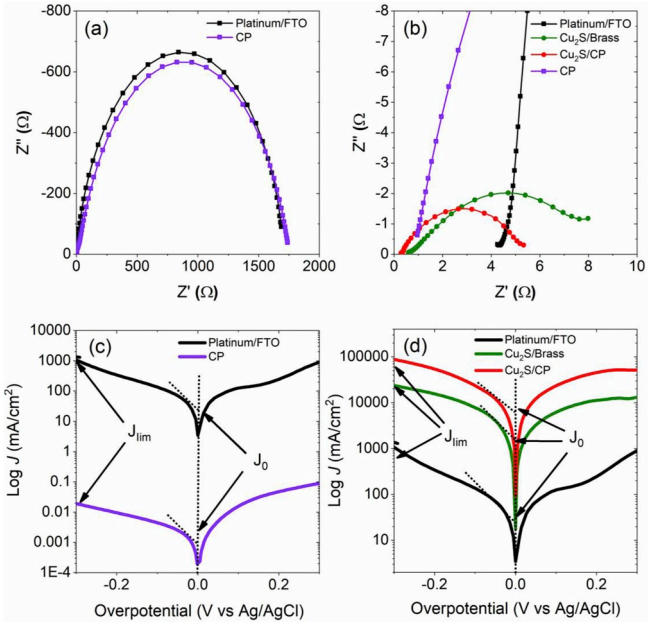

Fig. 5. Nyquist plots of symmetric cells: (a) Platinum/FTO (black square) and CP (violet square); (b) Platinum/FTO (black square), Cu_2S/Brass (green square), Cu_2S/CP (red square) and CP CEs (violet square). Tafel polarization curves using three-electrode configuration normalized with active areas of the CEs: (c) Platinum/FTO (black line) and CP (violet line); (d) Platinum/FTO (black line), Cu_2S/Brass (green line) and Cu_2S/CP (red line) CEs. (For interpretation of the references to color in this figure legend, the reader is referred to the Web version of this article.)

Table 1
Comparison of photovoltaic parameters calculated from J-V curves of CdS QDs sensitized QDSCs with Cu_2S/CP CEs prepared under different spray deposition conditions.

Types of CEs	J_{sc} (mA.cm^{-2})	V_{oc} (V)	*FF*	*PEC* (%)
One spray cycle	8.16	0.514	0.41	1.73
Two spray cycles	9.33	0.530	0.42	2.10
Three spray cycles	10.52	0.606	0.46	2.85
Four spray cycles	9.85	0.591	0.46	2.65

Table 2
Comparison of photovoltaic parameters of CdS QDs sensitized QDSCs with different types of CEs: Platinum/FTO; Cu_2S/Brass; CP and Cu_2S/CP (3-cycles) CEs.

Types of CEs	J_{sc} (mA.cm^{-2})	V_{oc} (V)	*FF*	*PEC* (%)
Platinum/FTO	6.25	0.511	0.23	0.73
Cu_2S/Brass	8.14	0.563	0.41	1.91
CP	4.51	0.503	0.28	0.63
Cu_2S/CP	10.52	0.606	0.46	2.85

parameters including short circuit current density [J_{sc} (mA cm^{-2})]; V_{oc} (V); *FF* and *PEC (%)* are reported in Table 1. QDSC with Cu_2S/CP CE with one spray cycle shows *PCE* of 1.73% with J_{sc} of 8.16 mA cm^{-2}; V_{oc} of 0.514 V; *FF* of 0.41 under one sun illumination. The performance of QDSCs escalates with the increase of the number spray deposition cycles of Cu_2S/CP CE and then decreases with further increase of spray cycles [Fig. 3 (c)- (d)].

Three spray deposition cycles Cu_2S/CP CE is the best performing CE and yields a *PCE* of 2.85%, which is 65% and 36% higher than the *PCE* of QDSCs with one and two spray cycles Cu_2S/CP CE respectively. However, QDSC based on four spray deposition cycles Cu_2S/CP CE shows lower performance as compared to three spray cycles Cu_2S/CP CE. This difference in the functional performance of QDSCs with different types of Cu_2S/CP CEs is mainly due to the different catalytic activity of the respective Cu_2S/CP CEs analysed by CV measurement.

We used CV to investigate the catalytic activity behaviour of the Cu_2S/CP CEs with different spray deposition conditions in relation to the obtained photovoltaic performance of QDSCs. Fig. 3 (a) displays a systematic comparison of CV of Cu_2S/CP CEs prepared by using different spray conditions. The calculated cathodic and anodic peaks current densities of Cu_2S/CP CEs with 3-cycles is highest as compared to Cu_2S/CP CEs with 4-cycles, 2-cycles and 1-cycle, indicating that 3-cycles of spray deposition for Cu_2S/CP CEs preparation yielding better catalytic activity, which is consistent with the obtained photovoltaic performance of QDSCs based on respective Cu_2S/CP CEs. In addition, another important parameter to evaluate the catalytic activity of different CEs, is the peak-to-peak separation (E_{PP}), that can be estimated from the CV measurements. The E_{pp} is inversely related to the standard electrochemical rate constant of a redox reaction [49]. The lowest value of E_{pp} of 0.450 mV for Cu_2S/CP CEs with 3-cycles is obtained as compared to Cu_2S/CP CEs with 4-cycles ($E_{pp} = 0.524$ mV), 2-cycles ($E_{pp} = 0.470$ mV) and 1-cycle ($E_{pp} = 0.570$ mV), which confirms the high catalytic activity of 3-cycles Cu_2S/CP CEs. The PV performance of Cu_2S/CP (PCE = 2.65%) CEs with 4-spray cycles is better than that of 2-spray cycles (PCE = 2.10%) although the E_{pp} of 4- spray cycles CE ($E_{pp} = 0.524$ mV) is higher than that of 2-spray cycles CEs ($E_{pp} = 0.470$ mV). This is may be due to difference in the amount of materials as well as the structural morphology of 2-spray cycles CEs compared to 4-spray cycles CEs (See Table 1S and Fig. 3S). This significant amount of Cu_2S materials grown through 4-spray cycles CEs yields a higher PCE than that of 2-spray cycles CEs. However, compared to the best performing 3-spray cycles Cu_2S/CP CEs, the formation of crack in the 4-spray cycles Cu_2S/CP CEs decreases performance [see Fig. 3S].

In addition, we used three electrode EIS measurements to evaluate the catalytic activities of Cu_2S/CP CEs under different spray deposition conditions. Tafel polarization curves of Cu_2S/CP CEs with different spray deposition conditions are shown in Fig. 6S. The exchange current density of CEs is directly related to the catalytic activity of CEs, which can be calculated from the intercepts of the extrapolated linear zone of the Tafel curves in the cathodic and anodic branches [50]. The calculated exchange current density of Cu_2S/CP CEs with different spray deposition conditions follows the trend 3-cycles > 4-cycles > 2-cycles > 1-cycle, which is consistent with the obtained photovoltaic performance of QDSCs based on respective CEs. This is also consistent with results obtained from CV measurements. Thus, 3-spray deposition cycles are the optimized conditions for best performing Cu_2S/CP CE.

After the optimization of spray deposition conditions, we performed a systematic comparison of the best performing 3-spray cycles Cu_2S/CP CEs with most commonly used Cu_2S/Brass [26,51–53] and Platinum/FTO [54,55] CEs for QDSCs. In addition, QDSCs were also fabricated by using CP CEs to highlight the specific contribution of CP and Cu_2S. Fig. 4 (a) displays the current density versus voltage curves of QDSCs fabricated by using five SILAR cycles CdS QDs sensitized TiO_2 anode with Cu_2S/CP, Cu_2S/Brass, Platinum/FTO and CP CEs. The calculated photovoltaics parameters of the respective QDSCs are reported in Table 2. The spray assisted Cu_2S/CP CE (3-cycles) yielding the highest *PCE* of 2.85% with $V_{oc} = 0.606$ V, $J_{sc} = 10.52$ mA cm^{-2} and $FF = 0.46$, whereas Cu_2S/Brass CEs, yielding the *PCE* of 1.91% with $V_{oc} = 0.563$ V, $J_{sc} = 8.14$ mA cm^{-2} and $FF = 0.41$. The QDSCs based on Platinum/FTO CE yielding the *PCE* of 0.73% with $V_{oc} = 0.511$ V, $J_{sc} = 6.25$ mA cm^{-2} and $FF = 0.23$. QDSCs based on CP CEs yield the lowest *PCE* of 0.63% with $V_{oc} = 0.503$ V, $J_{sc} = 4.51$ mA cm^{-2} and $FF = 0.28$. This significant difference in performance of QDSCs is mainly attributed to the catalytic behaviour difference of 3-spray cycles Cu_2S/CP CEs with Cu_2S/Brass, Platinum/FTO and CP CEs. In addition, to highlight the effect of the CP substrate, a systematic comparison of the photovoltaic performance of QDSCs based spray assisted 3-cycles Cu_2S CEs deposited on CP and FTO is shown in Fig. 8S and corresponding photovoltaic parameters is reported in Table 2S. QDSC with 3-cycles Cu_2S/CP CE is yielding the PEC of 2.85%, which is 26% higher than QDSC with Cu_2S/FTO CE [Fig. 8S **(a)**]. This is mainly attributed to better conductivity of CP substrate composed of a 3D network of carbon fibers as compared to the FTO.

The CV measurement of 3-cycles Cu_2S/CP, Cu_2S/Brass, Platinum/FTO and CP CEs are shown in Fig. 4 (b). The current densities of both anodic and cathodic peaks of 3-cycles Cu_2S/CP, Cu_2S/Brass, Platinum/FTO and CP CEs follow the trends: 3-cycles Cu_2S/CP > Cu_2S/Brass > Platinum/FTO > CP, demonstrate that Cu_2S/CP CE shows better catalytic activity than Cu_2S/Brass, Platinum/FTO and CP CEs. Similarly, the calculated E_{pp} values follow the trend 3-cycles Cu_2S/CP ($E_{pp} = 0.450$ mV) < Cu_2S/Brass ($E_{pp} = 0.540$ mV) < Platinum/FTO ($E_{pp} = 0.718$ mV) < CP ($E_{pp} = 0.725$ mV) CEs, confirming the higher catalytic activity of 3-cycles Cu_2S/CP CEs and is consistent with the obtained functional properties of QDSCs with these four types of CEs.

The stable electrocatalytic activity of the CEs is also an important factor to fabricate long-term stable QDSCs. The systematic comparison of electrocatalytic stability of Cu_2S/CP and the most commonly used Cu_2S/Brass CEs was assessed by measuring the 90 and 20 cycles of CV respectively, under similar experimental conditions (scan rate: 20 mV/s). The best performing Cu_2S/CP (3 cycles spray) CE shows a smaller drop in the oxidation (7.5%) and the reduction current density peaks (33.3%) after 90 cycles of CV [Fig. 4 (c)] compared to the oxidation (60%) and the reduction current density peaks (79%) of Cu_2S/Brass CE after only 20 cycles of CV [Fig. 4 (d)], which confirms that the Cu_2S/CP CE is more stable than the Cu_2S/Brass CE. The comparison of the oxidation and the reduction peaks of first and 90th CV cycles for Cu_2S/CP CE and first and 20th CV cycles for Cu_2S/Brass CE is shown in Fig. 7S. Du et al. reported the comparison of electrolytic catalytic stability of Cu_2S/FTO, activated carbon/Ti and mesoporous carbon/Ti CEs and demonstrated that the Cu_2S/FTO CEs show a significant decrease (51%) in the

current densities only after 5 cycles of consecutive measurements [56]. However, due to differences in the measurement conditions, in particular electrolyte concentration and scan rate significantly affect the variation in the current densities with the number of CV cycles. In addition, the long-term stable electrocatalytic activity of Cu_2S/CP is also confirmed by the comparison of long-term stability of QDSCs assembled by using different types of CEs: Cu_2S/CP and Cu_2S/Brass [Fig. 7].

3.3. Electrochemical impedance spectroscopy measurements

To further shed light on the catalytic activity of the different types of CEs and quantify the charge transfer resistance (R_{CT}) at the CE/electrolyte interface, EIS plots were recorded in a symmetric cell configuration, to eliminate the contribution of the TiO_2 photoanode [see Fig. 9S (**a**)]. In the symmetric configuration, two identical CEs (with the same active area of 0.25 cm^2) separated by a 25 μm spacer were filled with the same electrolyte used for all the solar cells. The R_{CT} in the electrolyte/catalyst is related to the reaction rate on the CEs, which is driven by its surface electro-catalytic activity. The Nyquist plots are reported in Fig. 5 (a)-(b), while the extrapolated parameters from the fitting of the data are reported in Table 3.

As previously observed, different equivalent circuits must be used to correctly describe the physical-chemical phenomena occurring at the CE with noble metals (e.g. platinum) [see Fig. 9S (**b**)] and semiconductors such as Cu_2S or Cu_2S/Brass [see Fig. 9S (**c**)] [47]. In particular, the main difference is the presence of the Nernst diffusion impedance element, Z_{W1} in the model for the semiconducting CEs. As visible in the Nyquist plots [Fig. 5 (a)-(b)] and in Table 3, the Platinum/FTO and simple CP-based CEs have the highest series resistance (R_s) and R_{CT}, confirming that platinum and simple CP are not suitable catalysts for QDSCs based on polysulfide electrolytes, as also observed in previous studies [47,57]. However, R_s of CP CE is lower than that of platinum/FTO CE. This may be due to the higher conductivity of the 3D network of the carbon fibers of the CP. In addition, the absence of a diffusion pattern confirms slow kinetics of the polysulfide reaction on the metal surface. Instead, the use of Cu_2S/Brass or Cu_2S as catalytic element for the CE increases drastically the reaction rate with a dramatic reduction of the R_{CT} compared to platinum-based CEs. These results are comparable to previous values reported in the literature [47,57].

In particular, the Cu_2S/Brass still outperforms all the other Cu_2S-based CEs. As previously observed, this can be related to the presence of metallic zinc on its surface [30,47]. Overall, these results would suggest that Cu_2S/Brass is a better choice than Cu_2S/CP due to the lower R_{CT}. However, the performance of the full device with Cu_2S/Brass CEs is not as good as that of those made with the spray assisted nanostructured Cu_2S/CP CEs. This highlights that the difference in morphology of the hierarchical structured Cu_2S/CP and Cu_2S/Brass CEs is a more dominant factor over the R_{CT} for the fast regeneration of the electrolyte during the device operation. Another possible explanation can be found by analyzing the values of the Nernst diffusion impedance element (Z_{W1}). By fitting the data of the high frequency arc it is possible to obtain the value of Z_{W1}: for the two cells, it increases in the order Cu_2S/CP < Cu_2S/Brass. This means that the diffusion coefficient (D) of S^{2-} ion for the different cells varies in the inverse order. In fact, Z_{W1} can be calculated by using the following equation [58–60]:

$$Z_{W1} = \frac{kT}{n^2 e_0^2 cA\sqrt{i\omega D}} \tanh^{-1}\left(\sqrt{\frac{i\omega}{D}}\delta\right)$$

where k is Boltzmann's constant, T is the absolute temperature, n is the number of electrons involved in the electrochemical reduction of S^{2-} at the electrode, e is the elementary charge, c is the concentration of S^{2-}, A is the electrode area, ω is the angular frequency of applied AC current and δ is the thickness of the diffusion layer. This result indicates that D increases with increasing electrocatalytic activity of the CE, confirming that the Cu_2S/CP CE with 3 cycles has the highest catalytic activity. The highest value of chemical capacitance (C_μ) is obtained for Cu_2S/CP CE with 3 cycles as compared to Cu_2S/Brass, Platinum/FTO and CP CEs (see Table 3). This is mainly attributed to the higher active surface area and larger amount of material loaded in Cu_2S/CP CE as compared to Cu_2S/Brass, Platinum/FTO and CP CEs.

The difference in catalytic activity of Platinum/FTO, Cu_2S/Brass and spray assisted Cu_2S/CP CEs can also be verified by the comparison of the exchange current density calculated from the Tafel polarization curves. Fig. 5 **(c)** and **(d)** show the Tafel polarization curves of Platinum/FTO, CP Cu_2S/Brass and spray assisted Cu_2S/CP CEs. The calculated exchange current density follows the trend Cu_2S/CP > Cu_2S/Brass > Platinum/FTO > CP CEs, which is consistent with the obtained photovoltaic performance of QDSCs based on the respective CEs. Thus, EIS measurements also confirmed the superior catalytic properties of spray assisted nanostructured Cu_2S/CP CEs (3-cycles) than Cu_2S/Brass, Platinum/FTO and CP CEs.

3.4. Superior photovoltaic performance of QDSCs based on cascade CdS/CdSe QDs

To further boost the performance of QDSCs, a well-known cascade CdS/CdSe QDs [61] co-sensitized TiO_2 mesoporous film is applied as photoanode due to broader absorption spectra as well as superior carrier dynamics properties with best performing Cu_2S/CP as CE. For this CdS/CdSe cascade QDs sensitization of the TiO_2 mesoporous film, initially five SILAR cycles of CdS were applied to TiO_2 mesoporous film and then 3 h CBD for CdSe growth and finally three SILAR cycles of ZnSe [45] (see more details in Experimental section). As a reference, QDSCs with similar photoanode configuration were also fabricated by using Cu_2S/Brass as CE.

Fig. 6 (a) shows the systematic comparison of current density versus voltage curves under one sun irradiation (AM 1.5 G, 100 mW cm^{-2}) for the QDSCs based on Cu_2S/CP and Cu_2S/Brass as CEs. The photovoltaic functional parameters of the corresponding devices are summarized in Table 4. The QDSC assembled with Cu_2S/CP CE attains a *PCE* of 5.06% (V_{oc} = 0.501 V, J_{sc} = 18.67 mA cm^{-2}, *FF* = 0.54), which is 28% higher than values for QDSCs based on Cu_2S/Brass CE (*PCE* = 3.98%, V_{oc} = 0.480 V, J_{sc} = 15.58 mA cm^{-2}, *FF* = 0.53) and is also higher than the PEC values reported in the literature for CdS/CdSe QDs co-sensitized QDSCs with different types of CEs (see Table 3S). This significant enhancement in the photovoltaic performance of QDSCs with Cu_2S/CP CEs compared to Cu_2S/Brass CEs is mainly ascribed to the superior electrocatalytic activity of Cu_2S/CP CE than its counterpart CE, as confirmed by CV and EIS measurements. The improved electrocatalytic activity of Cu_2S/CP CE enhances the rate of reduction of the oxidized electrolyte, which in turn speeds up QDs regeneration and hence the overall performance of QDSCs with Cu_2S/CP CE. These results are further supported by transient photovoltage decay measurements, discussed below. The QDSCs with cascade CdS/CdSe QDs co-sensitized TiO_2 mesoporous film photoanodes yield significantly higher PCE compared to CdS QDs sensitized TiO_2 mesoporous film photoanodes with both types of CEs (Cu_2S/CP and Cu_2S/Brass) due to broad absorption spectrum and effective carrier dynamics of cascade CdS/CdSe QDs as reported in the literature [26,62].

Transient photovoltage decay measurements were applied to gain

Table 3
Comparison of R_s (Ω), R_{CT} (Ω), Z_{w1} (Ω) and C (F.cm^{-2}) calculated from EIS measurements of symmetric cell configuration of Platinum/FTO, Cu_2S/Brass, CP and spray assisted Cu_2S/CP CEs.

Types of CEs	R_s (Ω)	R_{CT} (Ω)	Z_{w1} (Ω)	C_μ (F.cm^{-2})	β
Platinum/FTO	4.39	1651	–	6.95×10^{-05}	0.89
Cu_2S/Brass	0.59	0.261	7.93	1.69×10^{-04}	0.47
CP	0.93	1734	–	8.54×10^{-06}	0.80
Cu_2S/CP	0.31	3.76	1.25	1.14×10^{-02}	0.69

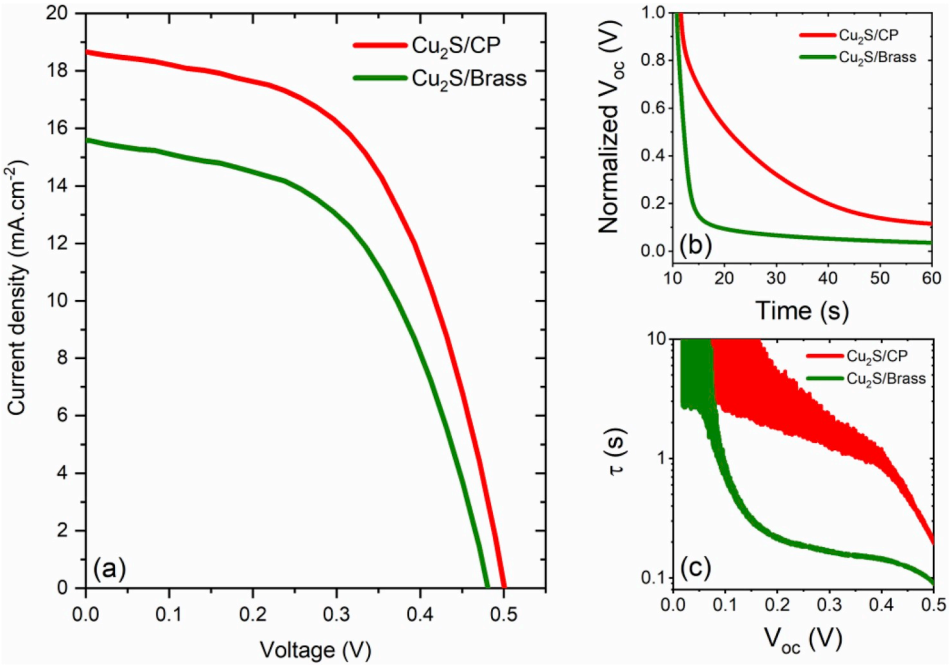

Fig. 6. (a) Current density vs voltage curves of QDSCs under one sun illumination based on different types of counter electrodes: red line (spray deposited Cu_2S/CP, 3 cycles) and green line (Cu_2S/Brass). Transient photovoltage decay measurements of corresponding QDSCs: (b) Normalized V_{oc} versus time (s); (c) calculated electron lifetime [τ (s)] versus V_{oc}. (For interpretation of the references to color in this figure legend, the reader is referred to the Web version of this article.)

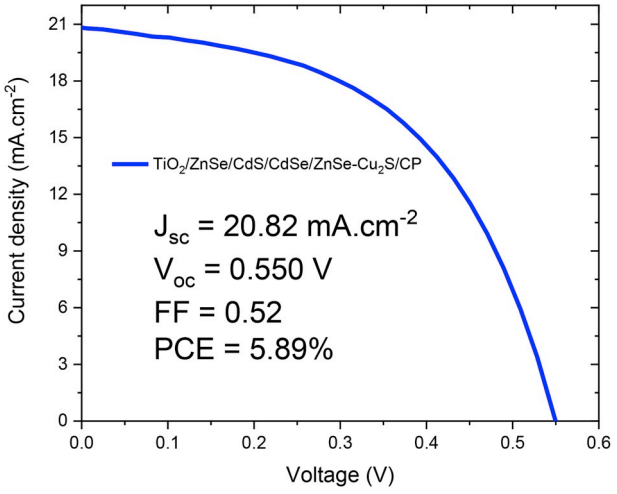

Fig. 7. Current density vs voltage curve of QDSC under one sun illumination based on TiO_2/ZnSe/CdS/CdSe/ZnSe photoanode and spray assisted Cu_2S/CP CE.

Table 4
Photovoltaic parameters of cascade CdS/CdSe co-sensitized QDSCs using spray assisted Cu_2S/CP (3-cycles) CEs and Cu_2S/Brass CEs as a reference.

Types of CEs	J_{sc} (mA.cm^{-2})	V_{oc} (V)	*FF*	*PEC* (%)
Cu_2S/CP	18.67	0.501	0.54	5.06
Cu_2S/Brass	15.58	0.480	0.53	3.98

insights into the carrier dynamics of the QDSCs with Cu_2S/CP and Cu_2S/Brass CEs. First, the QDSCs were illuminated under one sun simulated sunlight (AM 1.5, 100 mW cm^{-2}) until a steady state voltage was attained, which is the V_{oc} of the QDSCs. Then the simulator shutter was closed and the decay of V_{oc} with time was recorded under dark conditions. Fig. 6 (b) displays the comparison of the V_{oc} decay with time for the QDSCs with Cu_2S/CP and Cu_2S/Brass CEs. The rate of the V_{oc} decay is slower for the QDSCs with Cu_2S/CP CEs than the QDSCs with Cu_2S/Brass CEs [Fig. 6 (b)]. The calculated electron lifetime (τ) from the transient photovoltage decay measurements can be obtained by using the following equation [63,64]:

$$\tau = -\left(\frac{k_B T}{e}\right)\left(\frac{dV_{oc}}{dt}\right)^{-1}$$

where k_B is Boltzmann's constant, T is the absolute temperature, and e is the electronic charge.

Fig. 6 (c) displays the τ variation versus V_{oc}. The QDSC with Cu_2S/CP CE shows a longer value of τ as compared to QDSC with Cu_2S/Brass CE. At a particular V_{oc} (~0.400 V), the τ value is 0.142 s for QDSC with Cu_2S/Brass CE and 0.929 s for QDSC with Cu_2S/CP CE. This difference in the τ values is mainly attributed to lower carrier recombination in the QDSCs with Cu_2S/CP CE than QDSC with Cu_2S/Brass CE and is consistent with the obtained photovoltaic performance of the corresponding QDSCs [Fig. 6 (a)]. The long τ in QDSC with Cu_2S/CP CE confirms the increased collection of electrons and reduced carrier recombination. The latter leads to fast QDs regeneration by injecting electrons from the polysulfide redox couple electrolyte, which is reduced at the electrolyte/CE interface. The polysulfide redox couple electrolyte reduction rate is faster for Cu_2S/CP than Cu_2S/Brass CE as confirmed by the electrocatalytic activity obtained through CV and EIS measurements.

To further improve the performance of QDSCs based cascade CdS/CdSe co-sensitized TiO_2 mesoporous film with spray assisted Cu_2S/CP CE, we grew additional ZnSe layers prior to CdS/CdSe QDs deposition, while using the same device architecture as above. Fig. 7 displays the current density versus voltage curves of QDSCs based on TiO_2/ZnSe/CdS/CdSe/ZnSe photoanodes and spray assisted Cu_2S/CP CE.

All the photovoltaic parameters improve significantly with the addition of two ZnSe inner layers, while maintaining all other components the same. Briefly, with the addition of two ZnSe inner layers, J_{sc} increases from 18.67 to 20.82 mA cm^{-2}, V_{oc} increases from 0.501 to 0.550 V, and the PCE increases from 5.06 to 5.89%. This improvement is mainly attributed to the presence of the additional ZnSe inner layer,

which enhances the CdS/CdSe QDs loading on the TiO_2 mesoporous film consistent with the results reported by G. Cao et al. [65]. This high PCE of QDSCs with spray assisted Cu_2S/CP CEs highlights the potential application of Cu_2S/CP as an excellent CE.

3.5. Long-term stability measurements

The long-term stability is another important feature of the CEs, which plays a significant role in the overall stability of the QDSCs. Fig. 8 displays the systematic comparison of the QDSCs with Cu_2S/CP and with Cu_2S/Brass as CEs in terms of current density versus voltage curves [Fig. 8 (a)-(b)] and variation of the photovoltaic functional parameters versus time [Fig. 8 (c)-(f)]. Both QDSCs were characterized under one sun simulated sunlight (AM 1.5, 100 mW cm^{-2}) at room temperature and stored under ambient dark conditions after each measurement.

The QDSC with Cu_2S/CP CE shows better stability than the QDSC with Cu_2S/Brass CE tested for 490 min. Briefly, for the QDSC with Cu_2S/CP CE, J_{sc} increases from 11.68 to 12.33 mA cm^{-2} [Fig. 8 (e)], V_{oc} increases from 0.492 to 0.507 V [Fig. 8 (d)], *FF* increases from 0.44 to 0.48 [Fig. 8 (f)] and the *PCE* from 2.55 to 3.00% [Fig. 8 (c)] after 50 min since fabrication, due to better penetration of the electrolyte inside the TiO_2 mesoporous film. Similarly, for QDSC with Cu_2S/Brass CE, J_{sc} slightly increases from 9.84 to 9.96 mA cm^{-2} [Fig. 8 (e)], V_{oc} increases from 0.492 to 0.529 V [Fig. 8 (d)], and the *PCE* increases from 2.36 to 2.43% [Fig. 8 (c)], whereas *FF* decreases from 0.48 to 0.46 [Fig. 8 (f)] 50 min after fabrication. All the photovoltaic parameters of QDSCs based Cu_2S/CP and Cu_2S/Brass CEs decrease after 490 min of device fabrication. The rate of decrease in all photovoltaic functional parameters is higher for QDSCs with Cu_2S/Brass than QDSCs with Cu_2S/CP CE. After 490 min since fabrication, for QDSC with Cu_2S/Brass CE, the PCE decreases from 2.36 to 0.68% with significant decline of 71.18% [Fig. 8 (c)], whereas for QDSC with Cu_2S/CP, the *PCE* decreases only slightly from 2.55 to 2.48% with negligible decline of 2.71% [Fig. 8 (c)]. Similarly, after 490 min since fabrication, other photovoltaic parameters such as V_{oc} decreases from 0.492 to 0.402 V [Fig. 8 (d)], J_{sc} decreases from 9.84 to 3.67 mA cm^{-2} [Fig. 8 (e)], and *FF* decreases from 0.48 to 0.45 [Fig. 8 (f)] for QDSCs with Cu_2S/Brass CE, whereas for QDSC with Cu_2S/CP CE, V_{oc} slightly increases from 0.492 to 0.504 V [Fig. 8 (d)], J_{sc} decreases from 11.68 to 9.89 mA cm^{-2} [Fig. 8 (e)], and *FF* increases from 0.44 to 0.50 [Fig. 8 (f)]. This significant difference in long-term stability of QDSCs based on Cu_2S/CP and Cu_2S/Brass CEs is mainly attributed to better and stable electrocatalytic activity of Cu_2S/CP CE as compared to Cu_2S/Brass CE, which is confirmed by CV and EIS measurements. Also, the Cu_2S/Brass CE undergoes adverse corrosion effects on the brass substrate with polysulfide electrolyte [26,66,67], which reduces the long-term stability of the QDSCs. This corrosion issue of Cu_2S/Brass CE affects the photoanodes, as confirmed from the photograph of photoanodes (see Fig. 10S) with Cu_2S/Brass and Cu_2S/CP CEs 1440 min after fabrication. Thus, our spray deposited Cu_2S/CP CE shows remarkable electrocatalytic activity and long-term stability yielding highly efficient and stable QDSCs when compared with well-known Cu_2S/Brass CE.

4. Conclusion and perspectives

In summary, we have developed a simple, low cost and large area scalable spray deposition approach for the fabrication of nanostructured Cu_2S/CP CEs. CV and EIS measurements demonstrated that spray assisted Cu_2S/CP CEs posses better conductivity, stable catalytic activity and lower sheet resistance than that of conventional Cu_2S CEs prepared by treating brass with HCl. The QDSCs assembled with spray assisted nanostructured Cu_2S/CP CEs yield a PCE of 5.06%, which is 28% higher than QDSCs based Cu_2S/Brass as CEs and was further boosted to 5.89% upon optimization of the photoanode structure. In addition, QDSCs with spray assisted nanostructured Cu_2S/CP CEs shows better long-term stability than the QDSCs with Cu_2S/Brass CE. Thus, this excellent performance and satisfactory long-term stability for QDSCs with Cu_2S/CP CEs is mainly attributed to the synergistic effect of good conductivity of CP composed of a 3 D network of carbon fibers and high catalytic activity of nanostructured Cu_2S deposited on the CP. The results of this work offer a cost-effective and large area scalable approach to fabricate highly efficient and stable CEs, which is an important step toward the fabrication of solar driven opto-electric devices. Future directions will focus on the incorporation of carbonaceous materials in nanostructured Cu_2S/CP CEs to further boost the performance of the photoelectrochemical devices.

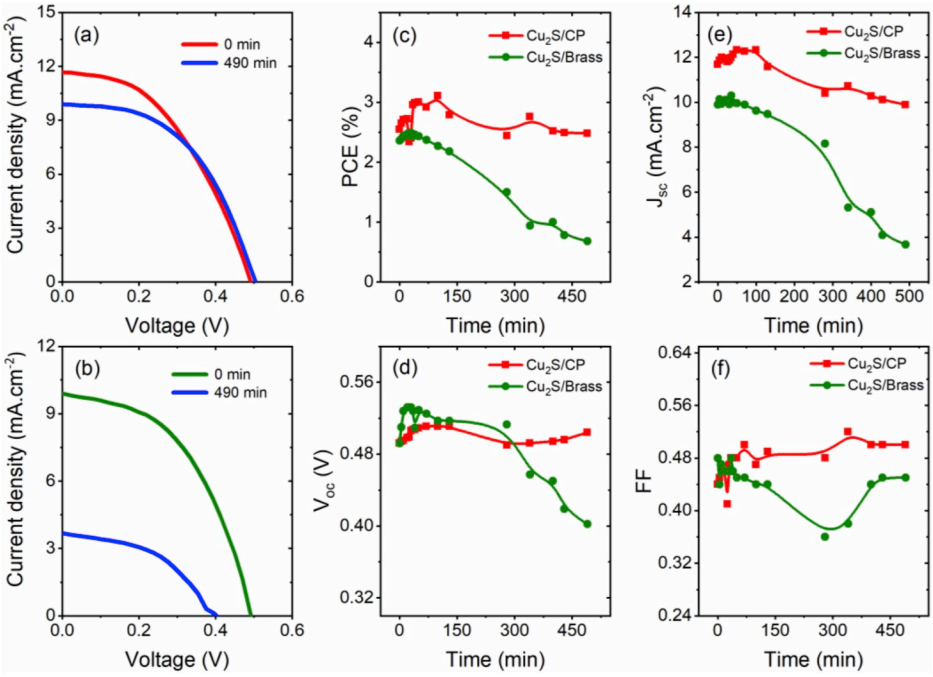

Fig. 8. Comparison of current density vs voltage curves of QDSCs at 0 min and after 490 min: (a) with spray assisted Cu_2S/CP CEs; (b) Cu_2S/Brass CEs. Variation of photovoltaic parameters of QDSCs based on spray assisted Cu_2S/CP (red square) and Cu_2S/Brass (green circle) CEs with time: (c) *PCE* (%); (d) V_{oc} (V); (e) J_{sc} (mA. cm^{-2}); (f) *FF*. (For interpretation of the references to color in this figure legend, the reader is referred to the Web version of this article.)

Acknowledgements

The authors acknowledge funding from the Natural Science and Engineering Research Council of Canada (NSERC, Discovery Grants) and the Canada Foundation for Innovation (CFI) for infrastructure and its operating funds. F.R. acknowledges partial salary support and funding from the Canada Research Chairs program. G.S.S. acknowledge the UNESCO Chair in MATECSS for a PDF Excellence Scholarship. M.M. is grateful to FRQNT for a PhD Scholarship (B2X). G.S.S and F.N.P. acknowledge funding from the University of Electronic Science and Technology of China and the China Postdoctoral Foundation. H. Zhao acknowledges start-up funds from Qingdao University. F.R. is grateful to the government of China for a Chang Jiang Scholar short-term award and to Sichuan province for a 1000 Talents Plan short-term award.

References

[1] S. Ruhle, M. Shalom, A. Zaban, Quantum-dot-sensitized solar cells, Chem. Phys. Chem 11 (2010) 2290–2304.
[2] Z. Pan, H. Rao, I. Mora-Seró, J. Bisquert, X. Zhong, Quantum-dot-sensitized solar cells, Chem. Soc. Rev. 47 (2018) 7659–7702.
[3] V.I. Klimov, Mechanisms for photogeneration and recombination of multiexcitons in semiconductor Nanocrystals: implications for lasing and solar energy conversion, J. Phys. Chem. B 110 (2006) 16827–16845.
[4] I. Moreels, Y. Justo, B. De Geyter, K. Haustraete, J.C. Martins, Z. Hens, Size-tunable, bright, and stable PbS quantum dots: a surface chemistry study, ACS Nano 5 (2011) 2004–2012.
[5] W.W. Yu, L.H. Qu, W.Z. Guo, X.G. Peng, Experimental determination of the extinction coefficient of CdTe, CdSe, and CdS nanocrystals, Chem. Mater. 15 (2003) 2854–2860.
[6] I.A. Ostapenko, G. Honig, C. Kindel, S. Rodt, A. Strittmatter, A. Hoffmann, D. Bimberg, Large internal dipole moment in InGaN/GaN quantum dots, Appl. Phys. Lett. 97 (2010), 063103.
[7] M.C. Beard, J.M. Luther, O.E. Semonin, A.J. Nozik, Third generation photovoltaics based on multiple exciton generation in quantum confined semiconductors, Acc. Chem. Res. 46 (2013) 1252–1260.
[8] A. Pandey, P. Guyot-Sionnest, Slow electron cooling in colloidal quantum dots, Science 322 (2008) 929–932.
[9] G.S. Selopal, H. Zhao, X. Tong, D. Benetti, F. Navarro-Pardo, Y. Zhou, Y.D. Barba, F. Vidal, Z.M. Wang, F. Rosei, Highly stable colloidal "giant" quantum dots sensitized solar cells, Adv. Funct. Mater. 27 (2017) 1701468.
[10] S. Jiao, Q. Shen, I. Mora-Sero, J. Wang, Z. Pan, K. Zhao, Y. Kuga, X. Zhong, J. Bisquert, Band engineering in core/shell ZnTe/CdSe for photovoltage and efficiency enhancement in exciplex quantum dot sensitized solar cells, ACS Nano 9 (2015) 908–915.
[11] J.Y. Kim, J. Yang, J.H. Yu, W. Baek, C.H. Lee, H.J. Son, T. Hyeon, M.J. Ko, Highly efficient copper–indium–selenide quantum dot solar cells: suppression of carrier recombination by controlled ZnS overlayers, ACS Nano 9 (2015) 11286–11295.
[12] V. Chakrapani, D. Baker, P.V. Kamat, Understanding the role of the sulfide redox couple (S^{2-}/S_n^{2-}) in quantum dot-sensitized solar cells, J. Am. Chem. Soc. 133 (2011) 9607–9615.
[13] Y.L. Liao, J. Zhang, W.G. Liu, W.X. Que, X.T. Yin, D.N. Zhang, L.H. Tang, W.D. He, Z.Y. Zhong, H.W. Zhang, Enhancing the efficiency of CdS quantum dot-sensitized solar cells *via* electrolyte engineering, Nano Energy 11 (2015) 88–95.
[14] Z.L. Du, Z.X. Pan, F. Fabregat-Santiago, K. Zhao, D.H. Long, H. Zhang, Y.X. Zhao, X. H. Zhong, J.S. Yu, J. Bisquert, Carbon counter-electrode-based quantum-dot-sensitized solar cells with certified efficiency exceeding 11%, J. Phys. Chem. Lett. 7 (2016) 3103–3111.
[15] S. Jiao, J. Du, Z.L. Du, D.H. Long, W.Y. Jiang, Z.X. Pan, Y. Li, X.H. Zhong, Nitrogen-doped mesoporous carbons as counter electrodes in quantum dot sensitized solar cells with a conversion efficiency exceeding 12%, J. Phys. Chem. Lett. 8 (2017) 559–564.
[16] H. Zhang, C. Yang, Z.L. Du, D.Y. Pan, X.H. Zhong, Graphene hydrogel-based counter electrode for high efficiency quantum dot-sensitized solar cells, J. Mater. Chem. 5 (2017) 1614–1622.
[17] (a) Z.L. Du, J. Tong, W.X. Guo, H. Zhang, X.H. Zhong, Cuprous sulfide on Ni foam as a counter electrode for flexible quantum dot sensitized solar cells, J. Mater. Chem. 4 (2016) 11754–11761;
(b) V.V. Chandu, M. Gopi, S. Singh, A.E. Reddy, H.-J. Kim, CNT@rGO@MoCuSe composite as an efficient counter electrode for quantum dot-sensitized solar cells, ACS Appl. Mater. Interfaces 10 (2018) 10036–10042.
[18] P.V. Kamat, J.A. Christians, J.G. Radich, Quantum dot solar cells: hole transfer as a limiting factor in boosting the photoconversion efficiency, Langmuir 30 (2014) 5716–5725.
[19] K. Meng, G. Chen, K.R. Thampi, Metal chalcogenides as counter electrode materials in quantum dot sensitized solar cells: a perspective, J. Mater. Chem. 3 (2015) 23074–23089.
[20] Y. Jiang, B.B. Yu, J. Liu, Z.H. Li, J.K. Sun, X.H. Zhong, J.S. Hu, W.G. Song, L. J. Wan, Boosting the open circuit voltage and fill factor of QDSSCs using hierarchically assembled ITO@Cu_2S nanowire array counter electrodes, Nano Lett. 15 (2015) 3088–3095.
[21] M.X. Wu, X. Lin, Y.D. Wang, T.L. Ma, Counter electrode materials combined with redox couples in dye- and quantum dot-sensitized solar cells, J. Mater. Chem. 3 (2015) 19638–19656.
[22] G. Hodes, J. Manassen, D. Cahen, Electrocatalytic electrodes for the polysulfide redox system, J. Electrochem. Soc. 127 (1980) 544–549.
[23] I. Concina, N. Memarian, G.S. Selopal, M.M. Natile, G. Sberveglieri, A. Vomiero, Spray-assisted SILAR deposition of cadmium sulphide quantum dots on metal oxide films for excitonic solar cells, J. Power Sources 240 (2013) 736–744.
[24] C.F. Wu, Z.X. Wu, J. Wei, H. Dong, Y.C. Gao, Improving the efficiency of quantum dots sensitized solar cell by using Pt counter electrode, ECS Electrochem. Lett. 2 (2013) 31–33.
[25] Y.L. Lee, Y.S. Lo, Highly efficient quantum-dot-sensitized solar cell based on Co-sensitization of CdS/CdSe, Adv. Funct. Mater. 19 (2009) 604–609.
[26] P.K. Santra, P.V. Kamat, Mn-doped quantum dot sensitized solar cells: a strategy to boost efficiency over 5%, J. Am. Chem. Soc. 134 (2012) 2508–2511.
[27] H.J. Yu, H.L. Bao, K. Zhao, Z.L. Du, H. Zhang, X.H. Zhong, Topotactically grown bismuth sulfide network film on substrate as low-cost counter electrodes for quantum dot-sensitized solar cells, J. Phys. Chem. C 118 (2014) 16602–16610.
[28] W.J. Ke, G.J. Fang, H.W. Lei, P.L. Qin, H. Tao, W. Zeng, J. Wang, X.Z. Zhao, An efficient and transparent copper sulfide nanosheet film counter electrode for bifacial quantum dot-sensitized solar cells, J. Power Sources 248 (2014) 809–815.
[29] G.S. Selopal, I. Concina, R. Milan, M.M. Natile, G. Sberveglieri, A. Vomiero, Hierarchical self-assembled Cu_2S nanostructures: fast and reproducible spray deposition of effective counter electrodes for high efficiency quantum dot solar cells, Nano Energy 6 (2014) 200–210.
[30] S. Wang, J. Tian, Recent advances in counter electrodes of quantum dot-sensitized solar cells, RSC Adv. 6 (2016) 90082.
[31] Z. Tachan, M. Shalom, I. Hod, S. Ruhle, S. Tirosh, A. Zaban, PbS as a highly catalytic counter electrode for polysulfide-based quantum dot solar cells, J. Phys. Chem. C 115 (2011) 6162–6166.
[32] S.X. Wang, T. Shen, H.W. Bai, B. Li, J.J. Tian, Cu_3Se_2 nanostructure as a counter electrode for high efficiency quantum dot-sensitized solar cells, J. Mater. Chem. C 4 (2016) 8020–8026.
[33] W.J. Ke, G.J. Fang, H. Tao, P.L. Qin, J. Wang, H.W. Lei, Q. Liu, X.Z. Zhao, In situ synthesis of NiS nanowall networks on Ni foam as a TCO-free counter electrode for dye-sensitized solar cells, ACS Appl. Mater. Interfaces 6 (2014) 5525–5530.
[34] D.H. Youn, M. Seol, J.Y. Kim, J.W. Jang, Y. Choi, K. Yong, J.S. Lee, TiN nanoparticles on CNT–graphene hybrid support as noble-metal-free counter electrode for quantum-dot-sensitized solar cells, Chem. Sus. Chem. 6 (2013) 261–267.
[35] Y.Y. Yang, L.F. Zhu, H.C. Sun, X.M. Huang, Y.H. Luo, D.M. Li, Q.B. Meng, Composite counter electrode based on nanoparticulate PbS and carbon black: towards quantum dot-sensitized solar cells with both high efficiency and stability, ACS Appl. Mater. Interfaces 4 (2012) 6162–6168.
[36] B. Fang, M. Kim, S.Q. Fan, J.H. Kim, D.P. Wilkinson, J. Ko, J.S. Yu, Facile synthesis of open mesoporous carbon nanofibers with tailored nanostructure as a highly efficient counter electrode in CdSe quantum-dot sensitized solar cells, J. Mater. Chem. 21 (2011) 8742–8748.
[37] S. Wang, B. Yang, H. Chen, E. Ruckenstein, Popgraphene: a new 2D planar carbon allotrope composed of 5–8–5 carbon rings for high performance lithium-ion battery anodes from bottom-up programming, J. Mater. Chem. 6 (2018) 6815–6821.
[38] D. Hou, W. Zhou, K. Zhou, Y. Zhou, J. Zhong, L. Yang, J. Lu, G. Li, S. Chen, Flexible and porous catalyst electrodes constructed by Co nanoparticles@nitrogen-doped graphene films for highly efficient hydrogen evolution, J. Mater. Chem. 3 (2015) 15962–15968.
[39] J.G. Radich, R. Dwyer, P.V. Kamat, Cu_2S reduced graphene oxide composite for high-efficiency quantum dot solar cells. Overcoming the redox limitations of S_{2-}/Sn_{2-} at the counter electrode, J. Phys. Chem. Lett. 219 (2011) 2453–2460.
[40] D. Ghosh, G. Halder, A. Sahasrabudhe, S. Bhattacharyya, A microwave synthesized Cu_xS and graphene oxide nanoribbon composite as a highly efficient counter electrode for quantum dot sensitized solar cells, Nanoscale 8 (2016) 10632–10641.
[41] D. Hou, W. Zhou, X. Liu, K. Zhou, J. Xie, G. Li, S. Chen, Pt nanoparticles/MoS_2 nanosheets/carbon fibers as efficient catalyst for the hydrogen evolution reaction, Electrochim. Acta 166 (2015) 26–31.
[42] Y. Zhang, C. Shi, X. Dai, F. Liu, X. Fang, J. Zhu, Pyrolysis preparation of Cu_2ZnSnS_4 thin film and its application to counter electrode in quantum dot-sensitized solar cells, Electrochim. Acta 118 (2014) 41–44.
[43] M.G. Ambia, M.N. Islam, M.O. Hakim, The effects of deposition variables on the spray pyrolysis of ZnO thin film, J. Mater. Sci. 29 (1994) 6575–6580.
[44] F. Huang, J. Hou, Q.F. Zhang, Y. Wang, R.C. Masse, S.L. Peng, H.L. Wang, J.S. Liu, G.Z. Cao, Doubling the power conversion efficiency in CdS/CdSe quantum dot sensitized solar cells with a ZnSe passivation layer, Nano Energy 26 (2016) 114–122.
[45] F. Huang, Q. Zhang, B. Xu, J. Hou, Wang, R.C. Masse, S. Peng, J. Liu, G.Z. Cao, Comparison of ZnS and ZnSe passivation layers on CdS/CdSe Co-sensitized quantum dot solar cells, J. Mater. Chem. 4 (2016) 14773–14780.
[46] G. Panzner, B. Egert, H.P. Schmidt, The stability of CuO and Cu_2O surfaces during argon sputtering studied by XPS and AES, Surf. Sci. 151 (1985) 400–408.

[47] R. Milan, M. Hassan, G.S. Selopal, L. Borgese, M.M. Natile, L.E. Depero, G. Sberveglieri, I. Concina, A player often neglected: electrochemical comprehensive analysis of counter electrodes for quantum dot solar cells, ACS Appl. Mater. Interfaces 8 (2016) 7766–7776.
[48] J.Y. Howe, C.J. Rawn, L.E. Jones, H. Ow, Improved crystallographic data for graphite, Powder Diffr. 18 (2003) 150–154.
[49] Q. Tang, H. Zhang, Y. Meng, B. He, L. Yu, Dissolution engineering of platinum alloy counter electrodes in dye-sensitized solar cells, Angew. Chem. Int. Ed. 54 (2015) 11448–11452.
[50] C.W. Kung, H.W. Chen, C.Y. Lin, K.C. Huang, R. Vittal, K.C. Ho, CoS acicular nanorod arrays for the counter electrode of an efficient dye-sensitized solar cell, ACS Nano 6 (2012) 7016–7025.
[51] J. Wang, I. Mora-Sero, Z.X. Pan, K. Zhao, H. Zhang, Y.Y. Feng, G. Yang, X.H. Zhong, J. Bisquert, Core/shell colloidal quantum dot exciplex states for the development of highly efficient quantum-dot-sensitized solar cells, J. Am. Chem. Soc. 135 (2013) 15913–15922.
[52] H. Zhang, K. Cheng, Y.M. Hou, Z. Fang, Z.X. Pan, W.J. Wu, J.L. Hua, X.H. Zhong, Efficient CdSe quantum dot-sensitized solar cells prepared by a post-synthesis assembly approach, Chem. Commun. 48 (2012) 11235–11237.
[53] M.A. Hossain, J.R. Jennings, C. Shen, J.H. Pan, Z.Y. Koh, N. Mathews, Q. Wang, CdSe-sensitized mesoscopic TiO_2 solar cells exhibiting >5% efficiency: redundancy of CdS buffer layer, J. Mater. Chem. 22 (2012) 16235–16242.
[54] S. Gimenez, I. Mora-Sero, L. Macor, N. Guijarro, T. Lana-Villarreal, R. Gomez, L. J. Diguna, Q. Shen, T. Toyoda, J. Bisquert, Improving the performance of colloidal quantum-dot-sensitized solar cells, Nanotechnology 20 (2009) 295204.
[55] K. Yan, L. Zhang, J. Qiu, Y. Qiu, Z. Zhu, J. Wang, S. Yang, A quasi-quantum well sensitized solar cell with accelerated charge separation and collection, J. Am. Chem. Soc. 135 (2013) 9531–9539.
[56] Z. Du, Z. Pan, F. Fabregat-Santiago, K. Zhao, D. Long, H. Zhang, Y. Zhao, X. Zhong, J.S. Yu, J. Bisquert, Carbon counter-electrode-based quantum-dot-sensitized solar cells with certified efficiency exceeding 11%, J. Phys. Chem. Lett. 16 (2016) 3103–3111.
[57] J.H. Zeng, D. Chen, Y.F. Wang, B.B. Jin, Graphite powder film-supported Cu_2S counter electrodes for quantum dot-sensitized solar cells, J. Mater. Chem. C 3 (2015) 12140–12148.
[58] F. Gong, H. Wang, X. Xu, G. Zhou, Z.S. Wang, In situ growth of $Co_{0.85}Se$ and $Ni_{0.85}Se$ on conductive substrates as high-performance counter electrodes for dye-sensitized solar cells, J. Am. Chem. Soc. 134 (2012) 10953–10958.
[59] A. Hauch, A. Georg, Diffusion in the electrolyte and charge-transfer reaction at the platinum electrode in dye-sensitized solar cells, electrochim, Acta 46 (2001) 3457–3466.
[60] F. Navarro-Pardo, L. Jin, R. Adhikari, X. Tong, D. Benetti, K. Basu, S. Vanka, H. G. Zhao, Z.T. Mi, S.H. Sun, V.M. Castano, A. Vomiero, F. Rosei, Nanofiber-supported CuS nanoplatelets as high efficiency counter electrodes for quantum dot-based photoelectrochemical hydrogen production, Mat. Chem. Front. 1 (2017) 65–72.
[61] Q. Wu, J. Hou, H. Zhao, Z. Liu, X. Yue, S. Peng, H. Cao, Charge recombination control for high efficiency CdS/CdSe quantum dot Co-sensitized solar cells with multi-ZnS layers, Dalton Trans. 47 (2018) 2214–2221.
[62] M.A. Becker, J.G. Radich, B.A. Bunker, P.V. Kamat, How does a SILAR CdSe film grow? Tuning the deposition steps to suppress interfacial charge recombination in solar cells, J. Phys. Chem. Lett. 5 (2014) 1575–1582.
[63] J. Bisquert, F. Fabregat-Santiago, I. Mora-Sero, G. Garcia-Belmonte, S. Gimenez, Electron lifetime in dye-sensitized solar cells: theory and interpretation of measurements, J. Phys. Chem. C 113 (2009) 17278–17290.
[64] A. Zaban, M. Greenshtein, J. Bisquert, Determination of the electron lifetime in nanocrystalline dye solar cells by open-circuit voltage decay measurements, Chem. Phys. Chem. 4 (2003) 859–864.
[65] F. Huang, L.S. Zhang, Q.F. Zhang, J. Hou, H.G. Wang, H.L. Wang, S.L. Peng, J. S. Liu, G.Z. Cao, High efficiency CdS/CdSe quantum dot sensitized solar cells with two ZnSe layers, ACS Appl. Mater. Inter. 8 (2016) 34482–34489.
[66] K. Zhao, H.J. Yu, H. Zhang, X.H. Zhong, Electroplating cuprous sulfide counter electrode for high-efficiency long-term stability quantum dot sensitized solar cells, J. Phys. Chem. C 118 (2014) 5683–5690.
[67] F.F. Wang, H. Dong, J.L. Pan, J.J. Li, Q. Li, D.S. Xu, One-step electrochemical deposition of hierarchical CuS nanostructures on conductive substrates as robust, high-performance counter electrodes for quantum-dot-sensitized solar cells, J. Phys. Chem. C 118 (2014) 19589–19598.